Fall 12-2-2011

Virtual Microstructure Generation of Asphaltic Mixtures

Mohammad Haft-Javaherian
University of Nebraska-Lincoln, mhjavaherian@huskers.unl.edu

VIRTUAL MICROSTRUCTURE GENERATION OF ASPHALTIC MIXTURES

by

Mohammad Haft-Javaherian

A THESIS

Presented to the Faculty of

The Graduate College at the University of Nebraska

In Partial Fulfillment of Requirements

For the Degree of Master of Science

Major: Civil Engineering

Under the Supervision of Professor Yong-Rak Kim

Lincoln, Nebraska

December, 2011

VIRTUAL MICROSTRUCTURE GENERATION OF ASPHALTIC MIXTURES

Mohammad Haft-Javaherian, M.S.

University of Nebraska, 2011

Adviser: Yong-Rak Kim

This thesis describes the development and application of a virtual microstructure generator incorporated with post-processing image analysis methods that can be used to fabricate a virtual, two-dimensional microstructure of asphaltic mixtures. In the generator, geometrical characteristics such as aggregate gradation, aggregate area fraction, angularity, orientation, and elongation were used to transform data from a three-dimensional (3D) mixture into its two-dimensional (2D) microstructure. The 2D virtual microstructures were generated from real 3D mixture information of asphaltic composites. Resulting virtual microstructures were then compared to real cross-sectional microstructure images obtained from actual samples for validation. Comparison presented a good agreement between the virtual and real microstructures, which demonstrates that the new 3D-2D transformation algorithms were properly developed and implemented into the virtual microstructure generator. Although much future work is required, the current development is at least sufficient to demonstrate the benefits and potential of this effort. Virtual fabrication and testing can result in significant time and cost savings compared to more expensive and repetitive laboratory fabrication and performance tests of actual specimens.

DEDICATION

To the savior of the world

ACKNOWLEDGMENTS

I would like to express my gratitude to my supervisor, Dr. Yong Rak kim, for his admirable guidance during this research, which contributed extensively to my education. His determination and focus on challenging research projects motivated me as a research assistant. I would like to thank my committee members, Dr. Maria Szerszen and Dr. Terry Stentz. I appreciate the contribution of their time and efforts.

I would like to thank my co-workers, Dr. Hoki Ban, Dr. Francisco Aragao, Dr. Jamilla Lutif, Mr. Soohyok Im, Mr. Pravat Karki, and Mr. Jun Zhang, for their support and productive conversations about our research topics. Thanks also go out to all friends that I made during this journey as a graduate student, especially Mr. Seyed Mahdi Alavizadeh for his support. Thanks are also due to the staff of the College of Engineering, of the Civil Engineering department and of the Nebraska Transportation Center (NTC).

I would like to express my heartfelt gratitude to my parents and my sister for their love and encouragement. Their love and support were greatly significant to give me strength to conclude this research.

TABLE OF CONTENTS

LIST OF FIGURES

LIST OF TABLES

CHAPTER 1

INTRODUCTION

To characterize the mechanical properties and performance behavior of asphaltic mixtures in pavement structures, mixture specimens have usually been fabricated and tested in the laboratory. This laboratory work is time-consuming and expensive, because it requires physical fabrication and testing of multiple specimens as well as equipment and devices. Therefore, to reduce the cost and time required to perform actual tests, researchers (Abbas et al. 2005; Song et al. 2006; You and Buttlar 2006; Dai and You 2007; Aragao and Kim 2010, 2011; Aragao et al. 2010, 2011; Karki 2010; Kim et al. 2010a; Aragao 2011; Lutif 2011) have pursued computational microstructure modeling approaches. Computational microstructure modeling is an appropriate way to predict the mechanical behavior of mixtures based on the proper characterization of the individual mixture constituents and their interactions in the mixtures. Computational microstructure modeling does not require a large number of expensive and time-consuming laboratory experiments because it typically relies on numerical techniques such as the finite element method (FEM) or discrete element method (DEM) on a mostly realistic scale and merely requires individual mixture constituent properties as model inputs.

Although computational microstructure modeling can significantly reduce the time and costs required to conduct mixture tests, it still requires the physical fabrication of mixture specimens and their further processes to obtain mixture microstructures. In two-dimensional (2D) modeling approaches, a digital image processing technique is usually necessary to treat surface images obtained from a mixture. As illustrated in Figure

1.1, after sample fabrication, the samples are sawn to form the physical 2D surface microstructure which is digitalized using electronic devices, such as scanners or digital cameras. The 2D raw image is then rendered in black and white to distinguish the multiple phases (such as asphalt and aggregates) in the mixture. The use of the digital image process has significantly improved the microstructure characterization and modeling of asphalt mixtures, but this method is also time consuming and labor intensive. Another issue is that the digital image processing technique is limited by the resolution of the digital image device, and is thus unable to capture the details of microstructure characteristics unless a very high resolution is adopted.

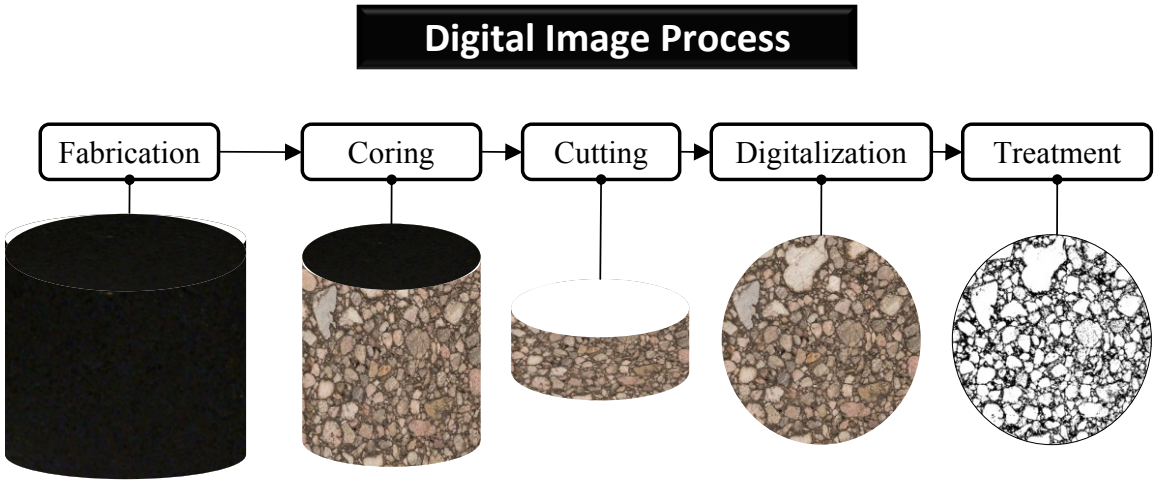

(a) physical microstructure fabrication

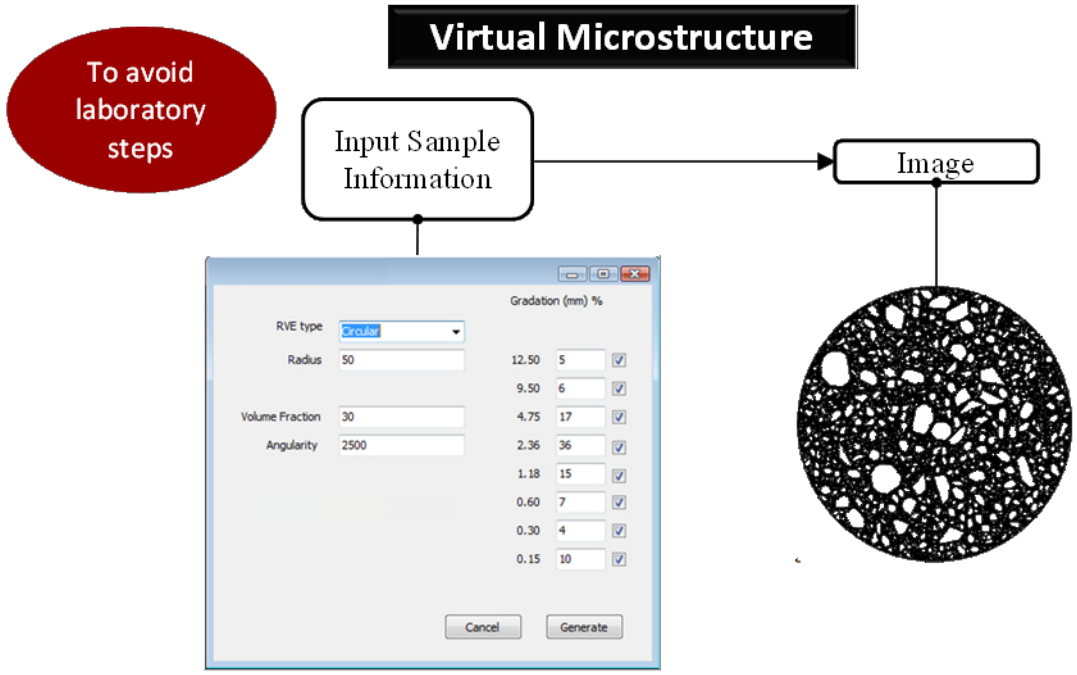

(b) virtual microstructure fabrication

Figure 1.1 Physical fabrication vs. virtual fabrication (Souza 2009).

Due to the limitations and practical drawbacks of computational modeling with physically obtained mixture microstructures, some researchers (Zhang 2003; Bullard et al. 2004; Stroeven et al. 2006; Souza 2009) have pursued virtual microstructure generation and its use for virtual laboratory testing. As illustrated in Figure 1.1, which

compares digital image processing of physical mixture microstructure and virtual microstructure generation, virtual microstructure generation is much faster and more cost-effective than digital image processing of physical microstructure. However, accurate algorithms are necessary in the process of virtual microstructure generation in order to obtain precise representations of the real mixtures.

The precise representation of the real microstructures through virtual computational generation is not a trivial task. In particular, composites such as asphaltic mixtures present significant heterogeneity due to aggregate particles that are irregularly-shaped, of different sizes, and randomly embedded in the asphaltic matrix. As illustrated in Figure 1.2, aggregates in a three-dimensional (3D) real sample can be misrepresented in an arbitrary 2D approximation. As can be seen in the figure, 2D images arbitrarily obtained from a cut 3D asphalt sample do not represent the same microstructure characteristics (in particular, the area fraction of particles and gradation of particles) due to somewhat unclear relationships between 3D and 2D. Therefore, the direct use of the volumetric mixture characteristics such as the 3D gradation from a typical aggregate sieve analysis, as an input to generate a 2D microstructure, is not appropriate. Zhang (2003) demonstrated in his dissertation that, when the 3D particle gradation is used to generate a 2D virtual microstructure, virtually generated 2D microstructures have many more large aggregate particles and larger particle density than 2D microstructures from cut surfaces of an actual 3D sample. This implies that volumetric aggregate gradation cannot be used directly to generate 2D virtual microstructures.

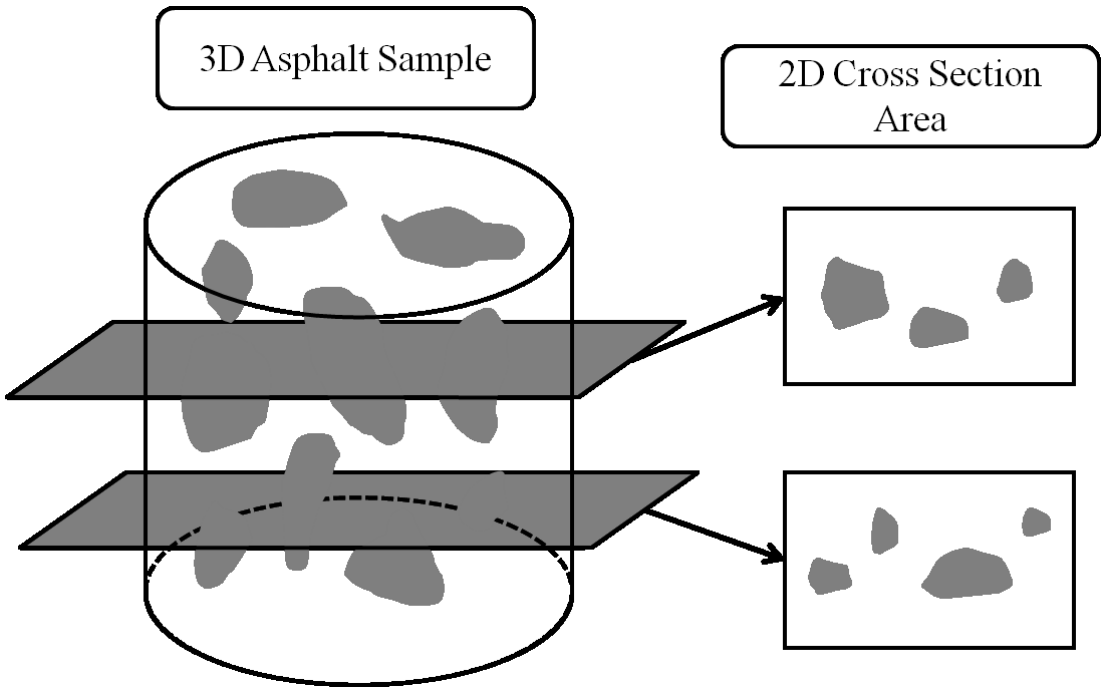

Figure 1.2 Difference between 3D and 2D aggregate representations (Zhang 2003).

To achieve the conversion from the actual 3D microstructure to its 2D representation in a more scientific manner, some studies (Higgins 2000; Zhang 2003; Hu and Stroeven 2006; Brandes and Hirata 2009; Souza 2009) have employed inverse stereology which is, as the name implies, the inverse process of general stereology. Stereology (Underwood 1970; Zhang 2003) is the process of predicting the 3D geometrical structure from 2D information, namely the geometry of cross-sections on several parallel planes. One of the most commonly used approaches is based on a statistical-geometrical approach; it measures a large number of 2D images to build up an actual picture of the average 3D structure. In an analogous manner, inverse stereology reconstructs the 2D cross-sections based on given 3D volumetric information. As illustrated in Figure 1.3, Zhang (2003) used the inverse stereology concept to convert the

3D volumetric microstructure into a 2D apparent microstructure in a cut surface. Generally, inverse stereology could improve virtual microstructure generation, but it still presents several limitations and challenges. The percent passing for 2D was always larger than that of 3D for the same sieve size, which means that there are more fine aggregates in 2D cut sections. Therefore, deviations in the aggregate gradation and area fraction between the virtual microstructure and physical microstructure exist, which become larger when one considers other geometric characteristics: angularity of aggregates, aspect ratio of aggregates, and orientation of aggregates in the mixture.

1.1. STUDY OBJECTIVES

The primary objective of this study is to develop an accurate, time-efficient, and lower-cost method for virtual microstructure generation of particulate composites in general, and of asphaltic mixtures in particular. Successful development of the method can potentially replace the physical sample fabrication and testing of mixture specimens, which is time-consuming and expensive. Some specific objectives of this study are as follows:

- To propose a rational method for converting 3D volumetric mixture gradation (which is known and given as an input) to 2D microstructure gradation;
- To propose a rational method for converting 3D volume fraction (which is known and given as an input) of each phase in the asphaltic mixture to 2D area fraction;
- To validate the newly developed methods by comparing the microstructure characteristics of virtual generations and actual microstructures from physical cuts of mixture samples.

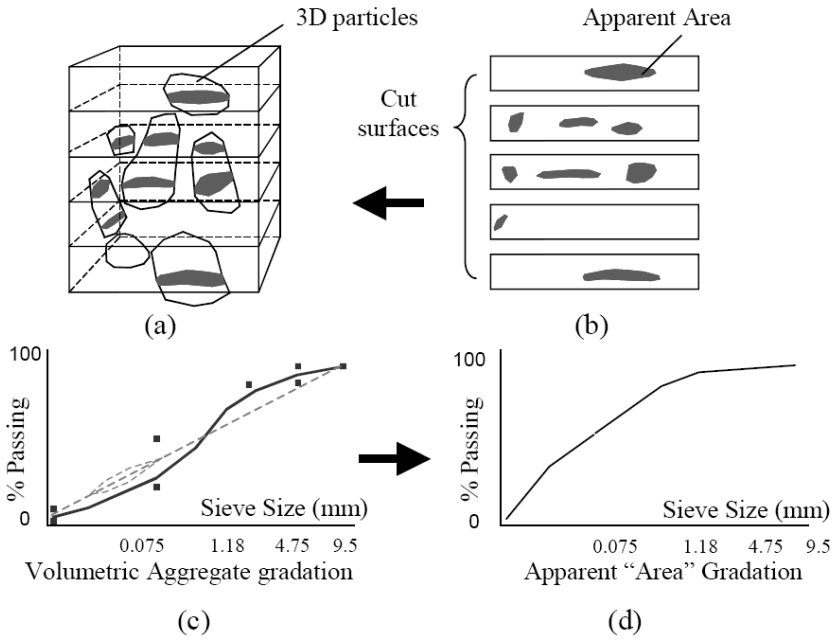

Figure 1.3 2D gradation through inverse stereology:
(a) 3D specimen; (b) 2D cut surfaces; (c) 3D gradation; (d) 2D gradation (Zhang 2003).

CHAPTER 2

VIRTUAL MICROSTRUCTURE GENERATION

Virtual microstructure generation as an alternative to physical fabrication is described in this chapter. Since the virtual specimen must imitate the geometrical characteristics of the actual specimen, virtual fabrication first utilizes the geometrical properties of aggregates, such as gradation, angularity, and aspect ratio. Then, the volume fraction and orientation of aggregates in the mixture are considered to appropriately represent aggregate particles in the mixture. As discussed in the following subsections, 3D to 2D conversion is necessary for the aggregate gradation and volume-area fraction, while other geometric characteristics (i.e., angularity, aspect ratio, and orientation) are based on 2D measurements and their statistical analysis results. Figure 2.1 summarizes how the virtual generation process is achieved in this study.

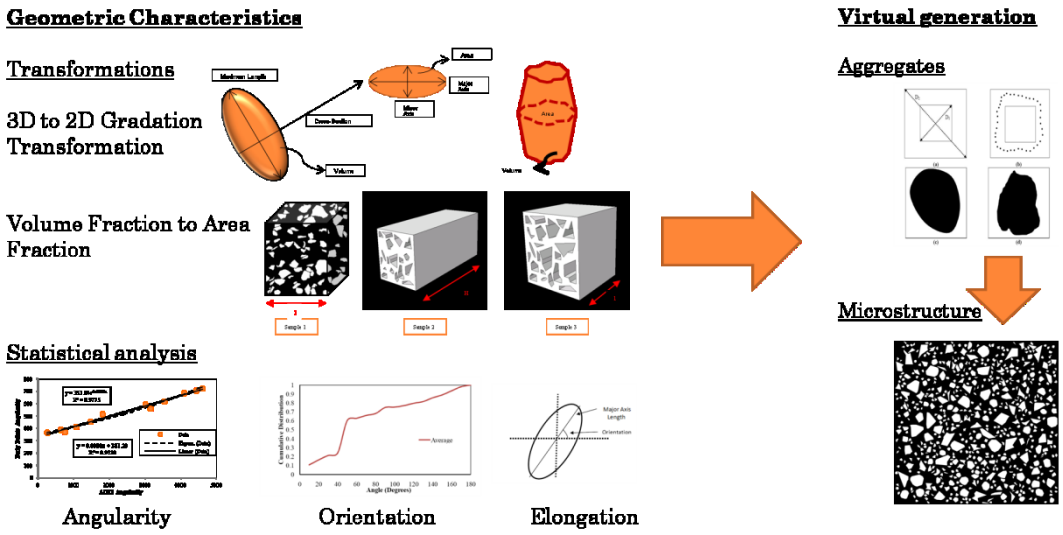

Figure 2.1 The virtual microstructure generation process employed in this study.

2.1. AGGREGATE GRADATION: 3D TO 2D TRANSFORMATION

Many studies have assumed, for simplicity, an equal third dimension for all the particles in the cross-section (Mora et al. 1998; Masad et al. 1999; Kwan et al. 1999; Marinoni et al. 2005; Brandes and Hirata 2009). However, this assumption is not clearly valid for the accurate transformation of asphaltic composites from 3D to 2D due to the irregular-shaped particles randomly embedded in the mixture. To improve the transformation accuracy, some other researchers (Higgins 2000; Zhang 2003; Bullard et al. 2004; Hu and Stroeven, 2006; Stroeven et al. 2006; Zelelew et al. 2008; Brandes and Hirata 2009; Souza 2009) have pursued different types of stereology methods, which certainly better represent the physics but remain limited in various ways.

3D aggregate particles in the mixtures present different 2D cross-sections based on different cutting planes. For instance, a 3D particle shown in Figure 2.2 is retained on standard sieve No. 8, but its two cross-sections (A-A and B-B) present different gradations. Thus, a proper transformation algorithm is necessary in the virtual generation process to convert the 3D gradation information into a 2D microstructure gradation when the mixture is a particulate composite in which particles with different sizes are randomly oriented in the mixture.

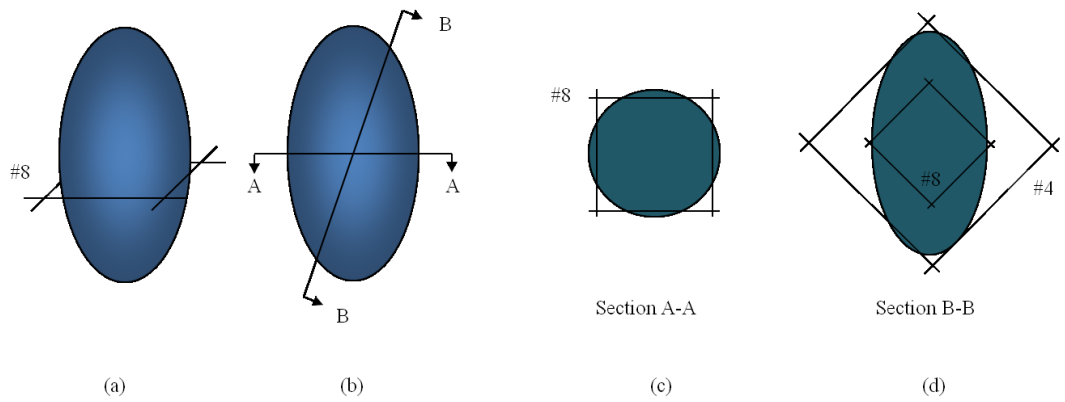

Figure 2.2 A 3D particle and its different cross-sections:
(a) the 3D particle and its 3D sieve size; (b) two different sections; (c) cross-section A-A; (d) cross-section B-B.

The 3D-2D gradation transformation method developed in this study is based on statistical simulation of individual aggregate particles that are defined by five imaginary geometric parameters (i.e., L, v, $l_{M,}$ $l_{m,}$ a).

As illustrated in Figure 2.3, an arbitrary aggregate particle is virtually generated with a maximum length (L) and volume (v). Then, the largest cross-section perpendicular to the maximum length can be defined by a major axis (l_M), minor axis (l_m), and an area (a). These five geometric characteristics defining an arbitrary particle are simulated by the following steps.

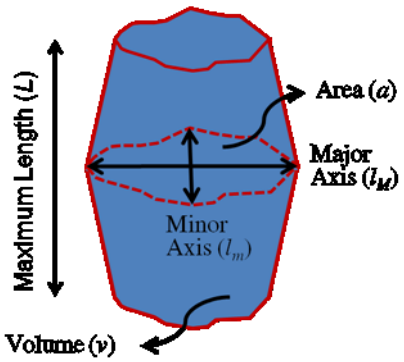

Figure 2.3. Five geometric characteristics defining an arbitrary aggregate particle.

Step 1: The maximum length (L) of the particle is generated randomly as a length between the diagonal distance of a sieve eye and the average maximum length of particles (*AMLP*) that are retained on the sieve. The *AMLP* is a physical quantity that can be measured from simple laboratory tests of aggregate particles. To conduct the whole process in a normalized manner, C-value, a ratio of *AMLP* to the sieve size (S), is introduced as follows:

$$C = \frac{AMLP}{S} \qquad [2.1]$$

Step 2: The major axis of the cross-section (l_M) is virtually generated as a random length between the diagonal lengths of two sequential sieve sizes to retain the particle on the smaller sieve, as illustrated in Figure 2.4.

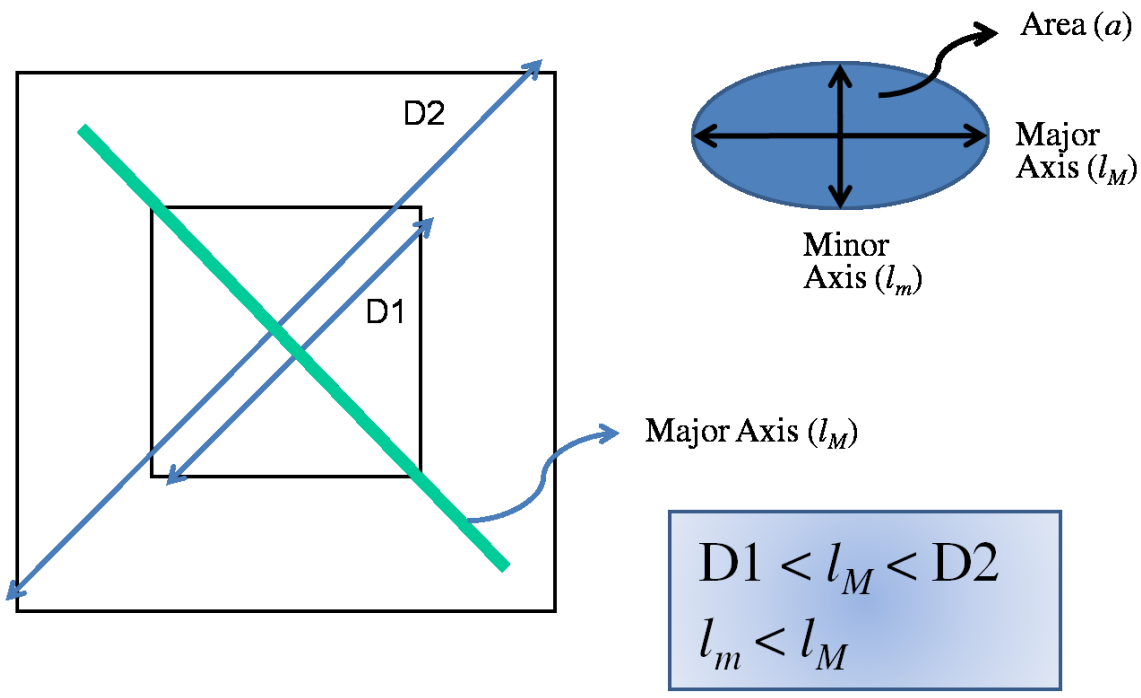

Figure 2.4 Major and minor axes in the cross-section of a randomly generated particle.

Step 3: The minor axis (l_m) of the cross-section, which is smaller than the major axis, is randomly generated as a length less than the major axis (l_M).

Step 4: The area (a) of the cross-section is a random area defined by a randomly generated ratio (r_a) multiplied by the area (a_r) of a reference cross-section (an ellipse with the same major and minor axes). Figure 2.5 illustrates this.

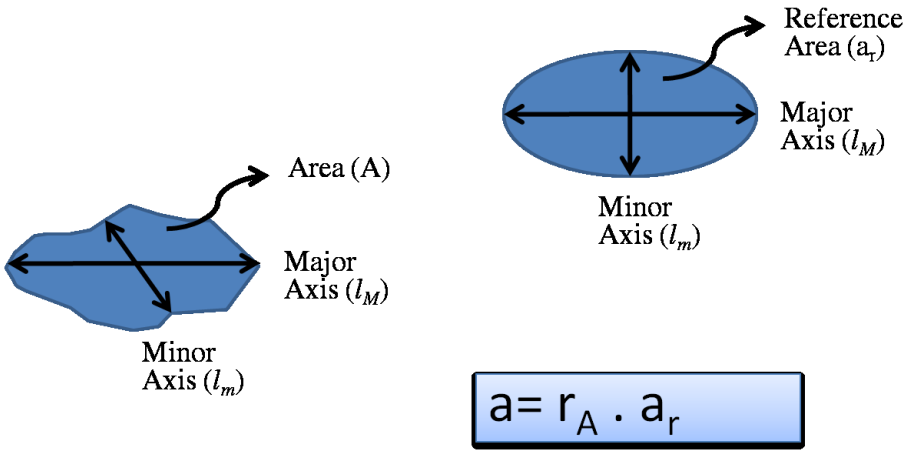

Figure 2.5 Area of a random particle and its reference cross-sectional area.

Step 5: Similar to Step 4, the volume (v) of the particle is a random volume defined by a randomly generated ratio (r_v) multiplied by the volume (v_r) of a reference object (a cylinder with the same cross-sectional area (a) and maximum length (L)). Figure 2.6 illustrates this.

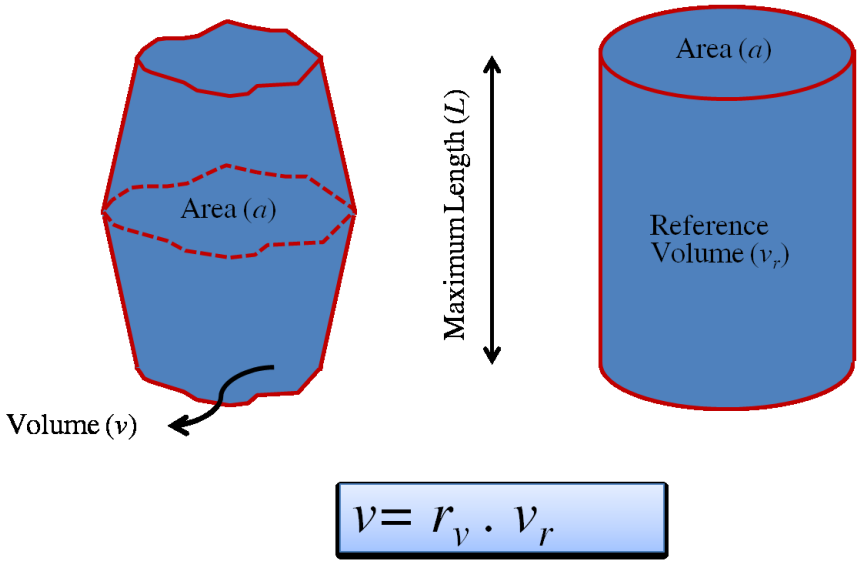

Figure 2.6 Volume of a random particle and its reference volume of an object.

Step 6: The 3D aggregate particle generated by the five random geometric parameters is cut to produce a random plane. The 2D gradation of the cut plane is then determined. This process is repeated in a large number of simulations for all different aggregates until a satisfactory level of statistical convergence is met for all sieve sizes. Through this computational simulation and resulting statistical analysis, the 2D gradation of a mixture can be obtained from the 3D mixture information. This 3D to 2D gradation transformation algorithm was implemented in the virtual microstructure generator.

2.2. AGGREGATE ANGULARITY: 3D TO 2D TRANSFORMATION

Aggregate angularity can be defined as the measurement of the sharpness of the corners of a particle. Thus, a rounded particle can be classified as a particle with low angularity and a non-rounded particle can be classified as a particle with high angularity. Figure 2.7 (Sukhwani et al. 2006) illustrates the geometric characteristics of an aggregate particle to help clarify the angularity and other shape features.

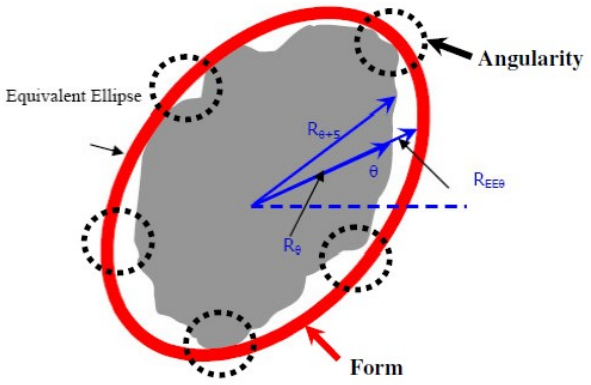

Figure 2.7 Geometric characteristics of an aggregate particle (Sukhwani et al. 2006).

Angularity can be estimated by gradient methods. The gradient method is based on the concept of gradient vectors. The direction of the gradient vector is used to calculate the measure of angularity of aggregate particles. In the gradient method, the direction of the gradient vector for adjacent points changes rapidly at the edge if the corners are sharp. On the other hand, the direction of the gradient vector changes slowly for adjacent points on the edge of the particle for rounded particles. Figure 2.8 exemplifies the concept with two cases: a rounded particle and an angular particle. Clearly, the change in the gradient vectors in the angular particle is much more rapid than the change from the rounded particle.

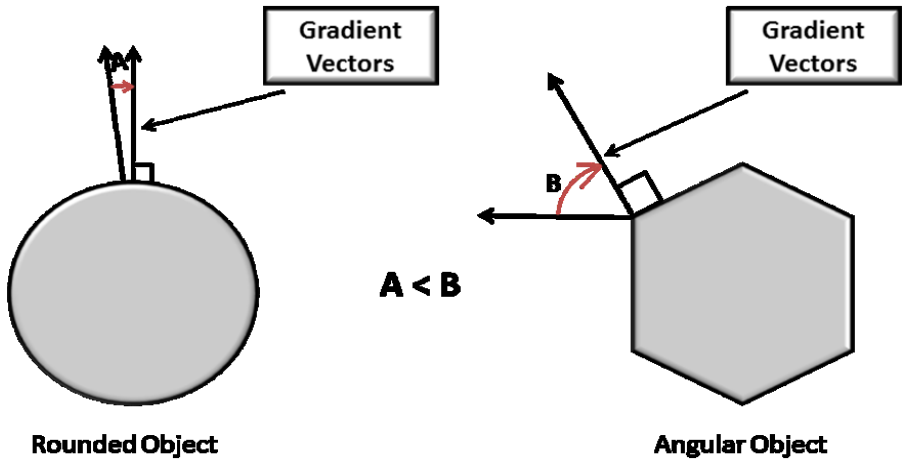

Figure 2.8 Gradient method to quantify aggregate angularity (Souza 2009).

Angles of the gradient vectors estimated at the total number of points on the edge of the particle are accumulated to finally produce the angularity index of the aggregate particle. The angularity index based on the gradient method (AI_G) is defined as follows (Masad 2004):

$$AI_G = \sum_{i=1}^{n-3} |\theta_i - \theta_{i+3}| \qquad [2.2]$$

where θ = angle of the gradient vector with the horizontal axis of the image;

i = the ith point on the edge of the particle; and

n = the total number of points on the edge of the particle.

As noted in Figure 2.8 and Equation [2.2], evaluation of aggregate angularity is based on the analysis of a 2D image of aggregates by monitoring differences among the gradient vectors at different edge points of the aggregate image. Therefore, the number of edge points selected affects the final value of angularity index.

The aggregate imaging system (AIMS), which is one of the approaches to characterize aggregate angularity, has been developed and popularly used by many researchers and practitioners. AIMS consists of a video microscope, video camera, data acquisition system, lighting system, automated carriage, and associated software. The aggregate particles are randomly spread on a disk tray. A video microscope is coupled with a black-and-white video camera to acquire images. The images are then analyzed to identify aggregates' geometric characteristics, including angularity, based on the gradient method.

The AIMS angularity index has been adopted by a previous study (Souza 2009) to represent aggregate sharpness in the mixture during the process of virtual microstructure generation. Sousa (2009) recommended using 40 edge points for angularity index calculation instead of the large number of points utilized in the AIMS method. He selected the number of points based on two limiting criteria: the image quality of the particles and computational efficiency in virtual microstructure generation. He found a

strong linear relationship between the AIMS angularity index and a 40-point angularity index, as demonstrated in Figure 2.9. This indicates that the use of 40 edge points in the virtual generation of aggregate particles in the 2D microstructure is approximate but sufficient to accurately represent realistic characteristics of aggregate angularity in actual mixtures. Based on this implication, this study also used the 40-point angularity index and resulting linear relationship in the conversion process from the actual angularity to the virtual angularity.

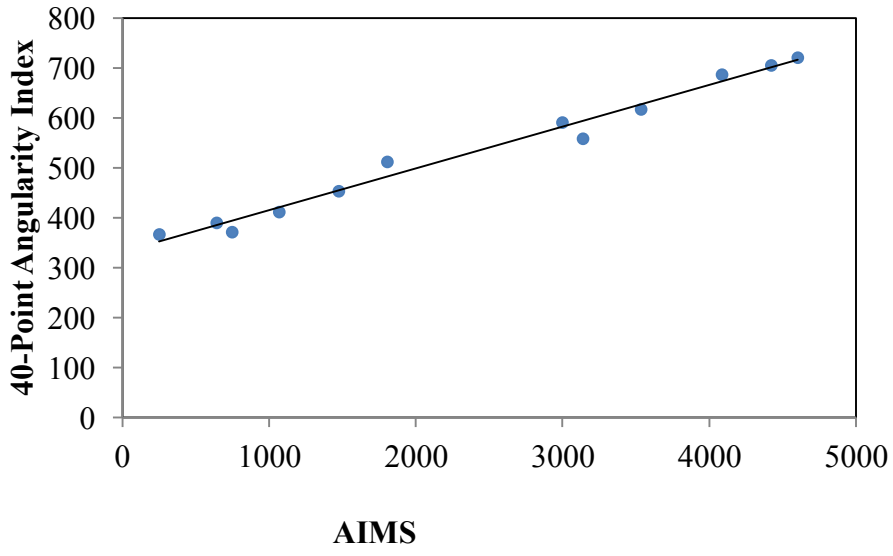

Figure 2.9 Relationship between AIMS angularity and 40-point angularity.

2.3. AGGREGATE ELONGATION: 3D TO 2D TRANSFORMATION

Among various indicators to characterize aggregate elongation, this study uses a simple indicator, aspect ratio (AR), which is defined in this study as the ratio of the major axis (l_M) to the minor axis (l_m) of a particle. Figure 2.10 illustrates the aspect ratio with two different cases: high elongation and low elongation.

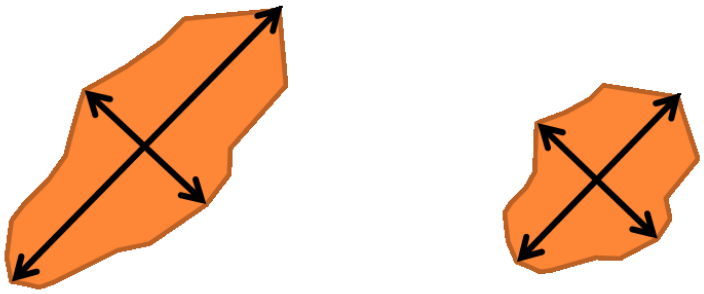

(a) (b)

Figure 2.10 Elongation by aspect ratio: (a) high elongation; (b) low elongation.

As mentioned earlier, when an aggregate particle is cut, its 2D representation can be different from the original 3D form. Therefore, 2D aggregates obtained from the cut planes may result in different aspect ratios because they are dependent on several factors, including particle shape and cutting directions. Such dependence is not only complex but also highly mixture specific; thus, the best practical approach is probably to use a digital image technique and a corresponding statistical analysis of cut planes obtained from some representative mixtures. To that end, Souza (2009) selected three different mixtures (two dense-graded mixtures with different nominal maximum aggregate sizes (NMAS) and one gap-graded mixture) and conducted image analyses of several cut planes taken from individual mixtures. From the image analysis, it has been noticed that the aspect ratio is mostly between 1 and 2, although the elongation trend depends somewhat on the size of aggregates in the mixture. Based on this finding, and for simplicity, the elongation parameter (i.e., aspect ratio *AR*) was implemented in the virtual microstructure generator in such a way that the aggregates are randomly elongated up to twice their width following a uniform random distribution.

2.3. TRANSFORMATION: 3D VOLUME FRACTION TO 2D AREA FRACTION

Similar studies (Zhang 2003; Souza 2009) have assumed that the 2D area fraction (*AF*) of aggregates is equal to the 3D volume fraction (*VF*). Since the aggregate particles are in random 3D shapes and present different cut surfaces, such a simple assumption cannot be made. Therefore, in this study, a new transformation method from the *VF* to *AF* is developed, as expressed by the following steps.

Step 1: The original 3D mixture sample (denoted hereafter as the first sample), a unit cube ($1 \times 1 \times 1$), is transformed to a new 3D mixture sample (denoted hereafter as the second sample). As shown in Figure 2.11, the second sample is prismatic ($1 \times 1 \times h$) with a constant unit square cross-section. Aggregate particles in the first sample are also transformed to prismatic bars in the second sample with the same volume fraction of aggregates. Since the aggregates in the second sample are prismatic bars, the *AF* of aggregates in the second sample (i.e., AF_2) is equal to the *VF* of the second sample (VF_2) and the *VF* of the first sample (VF_1). Correspondingly, the resulting height (h) of the second sample does not affect the *AF* and *VF*. In addition, because the first sample is a unit cube, the aggregate *VF* of the first sample (VF_1) is the same as the volume of aggregates in the first sample (V_1), and the aggregate *AF* of the second sample (AF_2) is equal to the cross-sectional area of aggregates in the second sample (A_2). All of these relations are summarized in Equation [2.3].

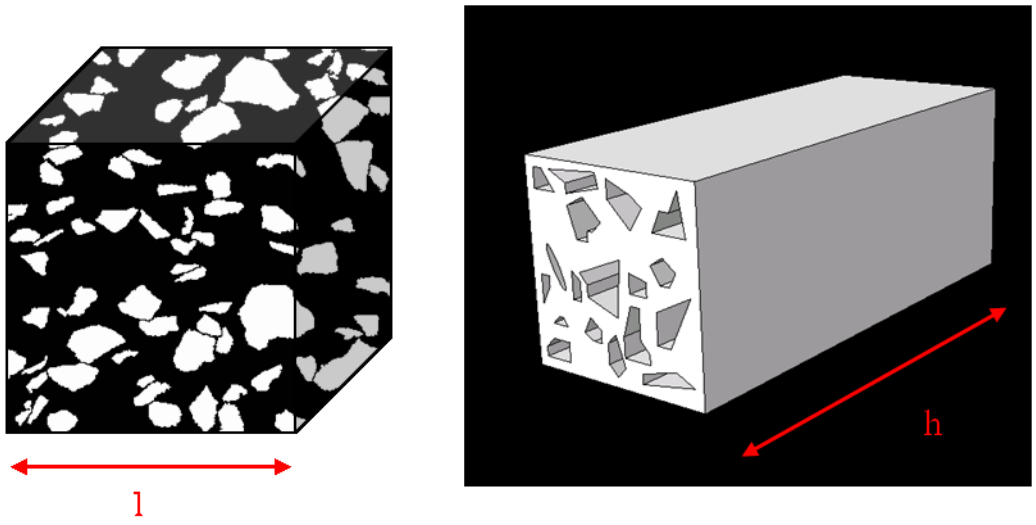

(a) (b)

Figure 2.11 Transformation from (a) original sample (first sample) to (b) second sample.

$$V_1 = VF_1 = VF_2 = AF_2 = A_2 \qquad [2.3]$$

where, V_1 = volume of aggregates in the first (original) sample;

VF_1 = VF of aggregates in the first sample;

VF_2 = VF of aggregates in the second sample;

AF_2 = AF of aggregates in the second sample; and

A_2 = area of aggregates on the cross-section of the second sample.

The h-value of the second sample can be estimated from the gradation transformation discussed earlier: Section 2.1. To make this estimation, all of the simulated particles in the gradation transformation process are first transformed to prismatic bars with the same cross-sectional areas. Then, a quantity (α) is obtained by dividing the volumes of all simulated particles by the areas of their cross-sections.

$$\alpha = \frac{\sum_{i=1}^{n} v_i}{\sum_{i=1}^{n} a_i} \qquad [2.4]$$

where, α = average height of all particles;

v_i = volume of ith particle simulated;

a_i = area of ith particle simulated; and

n = total number of particles simulated.

The h-value is then calculated by multiplying the α-value by the aggregate volume fraction of the second sample, VF_2 as follows:

$$h = \alpha \times VF_2 \qquad [2.5]$$

Step 2: In this step, the second prismatic sample is transformed to another prismatic sample (denoted hereafter as the third sample) with unit height (1 × 1 × 1), as illustrated in Figure 2.12. The same volume of aggregates in the second sample is maintained for the third sample; thus, the cross-sectional area of aggregates of the third sample is different from the cross-sectional aggregate area of the second sample. Through this second transformation, the following relationship can be written:

$$V_3 = A_3 \times 1 = V_2 = A_2 \times h \qquad [2.6]$$

where, V_3 = volume of aggregates in the third sample; and

A_3 = area of aggregates on the cross-section of the third sample.

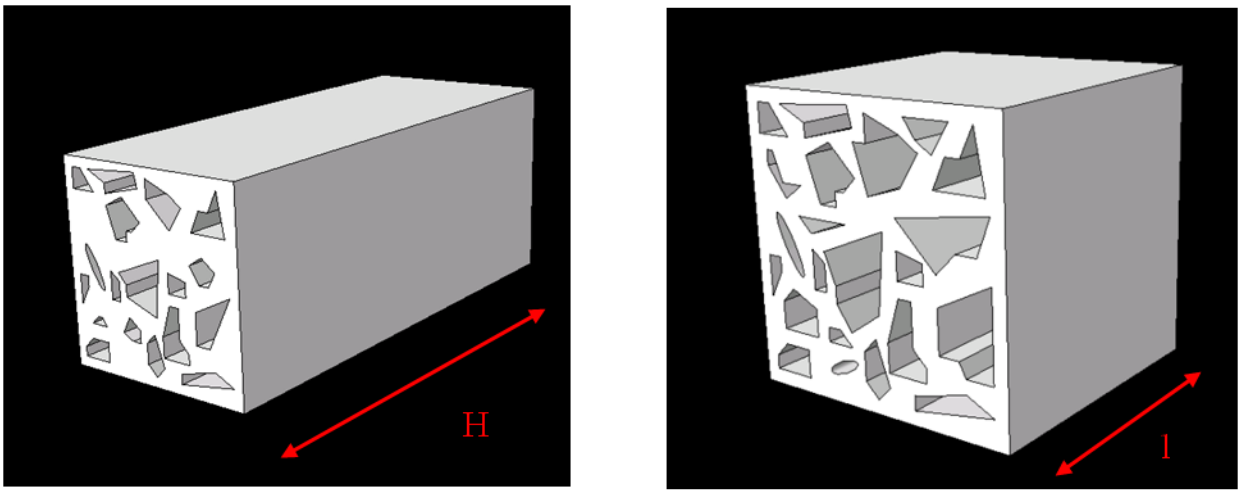

(a) (b)

Figure 2.12 Transformation from (a) second sample to (b) third sample.

Combining Equations [2.3], [2.5], and [2.6] yields the following relationship:

$$A_3 = \alpha \times (VF_2)^2 \qquad [2.7]$$

Since the aggregates in the third sample are also prismatic bars embedded in a unit square cross-section, the *AF* of aggregates in the third sample (i.e., AF_3) is equal to the cross-sectional area of aggregates in the third sample (A_3). With this relationship and the relationship in Equation [2.3] indicating that the aggregate volume fraction of the second sample (VF_2) is equal to the aggregate volume fraction of the original sample (VF_1), the following equation linking VF_1 to AF_3 can be written as follows:

$$A_3 = \alpha \times (VF_2)^2 = AF_3 = \alpha \times (VF_1)^2 \qquad [2.8]$$

Equation [2.8] implies that the aggregate *AF* necessary to achieve the 2D virtual microstructure generation can be simply estimated by the aggregate *VF* of the actual 3D mixture and the α-value which is obtained from the particle simulations in the process of 3D-2D gradation transformation. This 3D volume to 2D area transformation algorithm was implemented in the virtual microstructure generator.

2.4. AGGREGATE ORIENTATION: 3D TO 2D TRANSFORMATION

Aggregate orientation can be determined by measuring the angle between the major axis of each aggregate and a horizontal line, which ranges from 0^o to 180^o, as illustrated in Figure 2.13 (Zhang 2003). It is commonly accepted that aggregates in asphalt mixtures are randomly oriented; however, the compaction process might induce preferred orientation, as several studies (Zhang, 2003; Souza, 2009) have demonstrated.

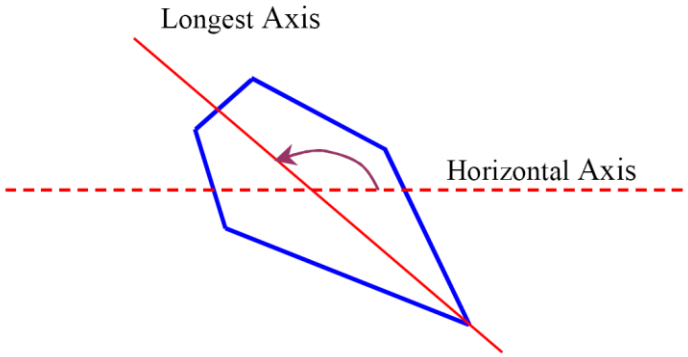

Figure 2.13 Definition of aggrerate orientation (Zhang 2003).

Similar to other geometric factors discussed earlier, 2D aggregates observed from cut planes of asphalt mixture samples present orientation characteristics different from their actual 3D aggregate particles in the mixtures as a result of several factors, including particle shape and cutting directions. Such dependence is not easy to identify and also

highly mixture specific. Therefore, as pursued in the analysis of particle aspect ratio, the digital image technique and corresponding statistical analysis of cut planes obtained from several representative asphalt mixtures was conducted by Souza (2009). He selected three different mixtures (i.e., two dense-graded mixtures with 9.5-mm NMAS and 12.5-mm NMAS, respectively, and one gap-graded SMA mixture) and conducted image analyses of multiple cut planes taken from individual mixtures. Figure 2.14 shows analysis results of the aggregate orientation. As can be seen in the figure, aggregates of all three types of mixture follow a similar trend, having a very clear concentration of aggregates with an orientation angle between 40^{o} and 50^{o}.

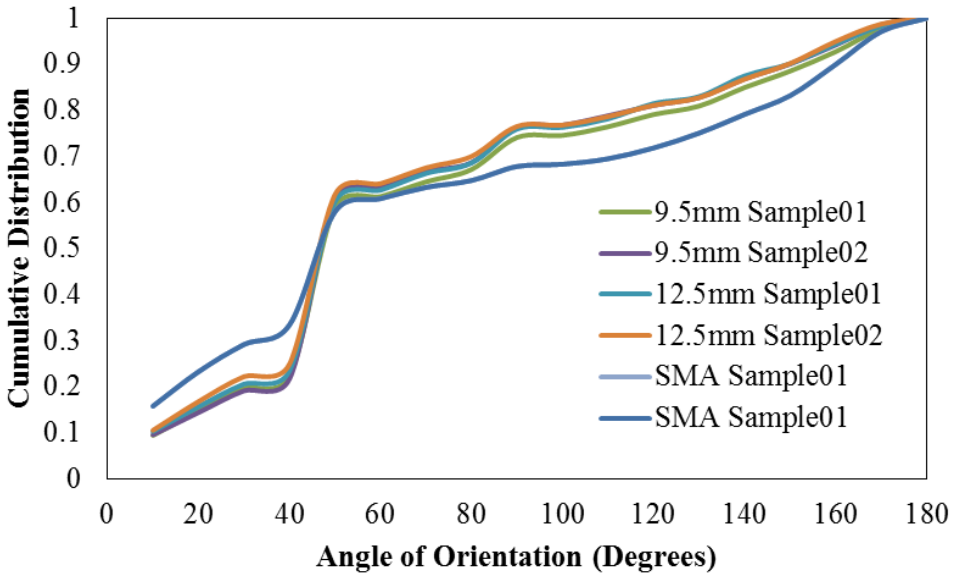

Figure 2.14 Analysis results of aggregate orientation from three different mixtures.

Based on the finding by Souza (2003), and for simplicity, the average cumulative distribution curve presented in Figure 2.15 was implemented in the virtual microstructure generator to represent the orientation characteristics of aggregates.

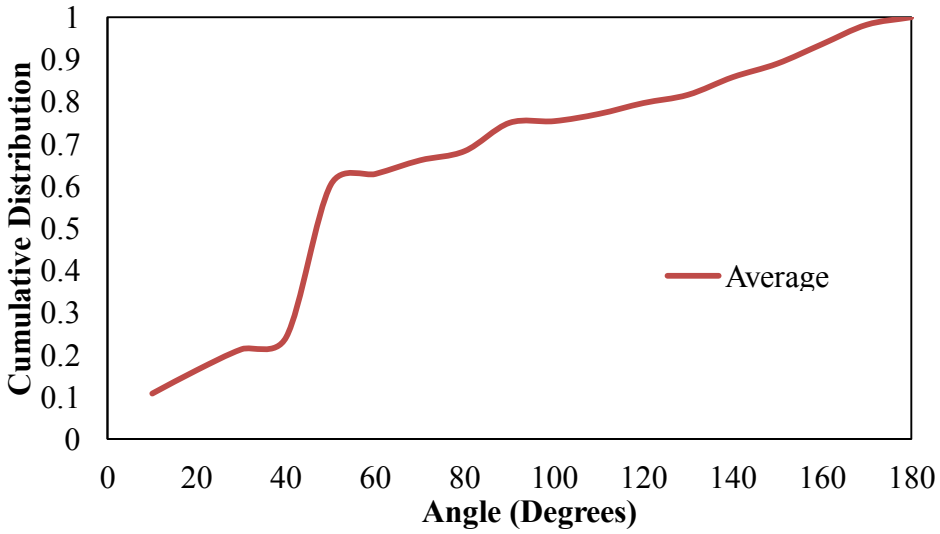

Figure 2.15 Average cumulative distribution curve of aggregate orientation.

2.1. COMPUTATIONAL GENERATION OF VIRTUAL MICROSTRUCTURE

Based on the 3D gradation, 3D volume fraction, orientation, elongation, and angularity, the virtual 2D aggregates are generated and embedded in the virtual mixture. To generate each particle retained on a specific sieve but passing one larger sieve, 40 points are placed between two squares in which the edge of the inner square is equal to the eye width of the smaller sieve size, and the edge of the outer square is equal to the eye width of the next consecutive larger sieve size. This process is illustrated in Figure 2.16(a) and 2.16(b). In order to control the angularity of the particle, the 40 points are interpolated by different types of splines to obtain the target angularity, which is illustrated in Figure 2.16(c) and 2.16(d).

Subsequently, the aggregate is elongated, rotated, and finally randomly placed in the virtual 2D sample area. When the aggregate is placed, overlapping with other aggregates that have already been placed is checked. When overlapping occurs, the aggregate is placed in a different location. This process continues until all aggregates are

generated to meet their target values of gradation and volume fraction. Aggregate generation starts from the largest and proceeds to the smallest sieve size. Figure 2.17 illustrates the steps (or algorithm) conducted to complete the virtual microstructure generation in a form of flowchart.

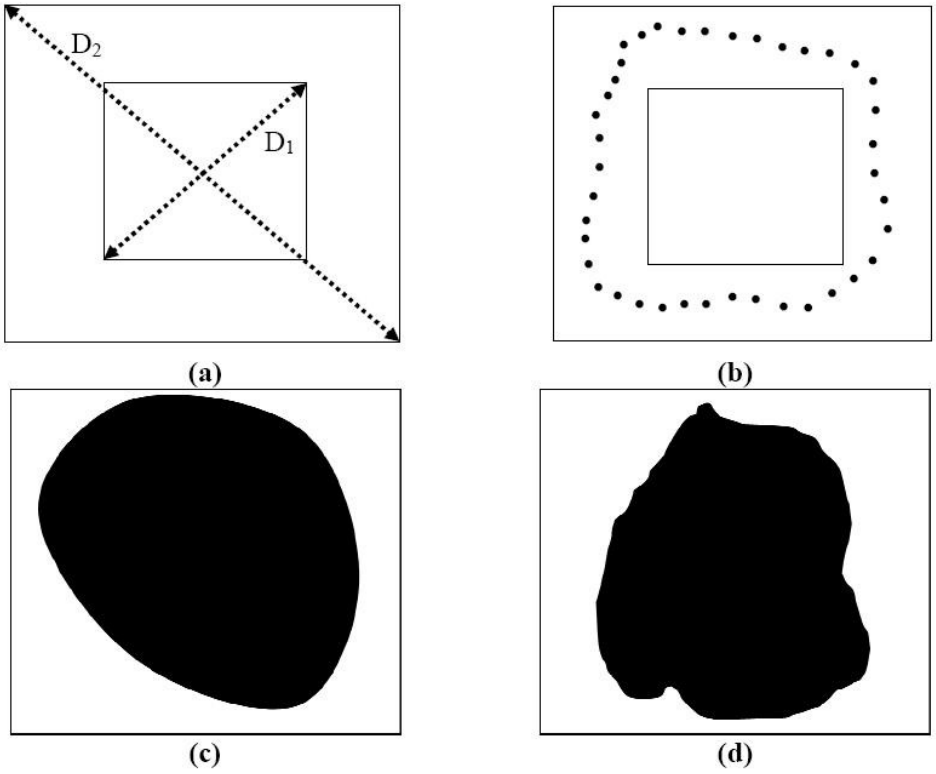

Figure 2.16 Aggregate generation process:
(a) two consecutive sieves; (b) 40 points randomly placed between the two sieves; (c) smooth aggregate; (d) angular aggregate.

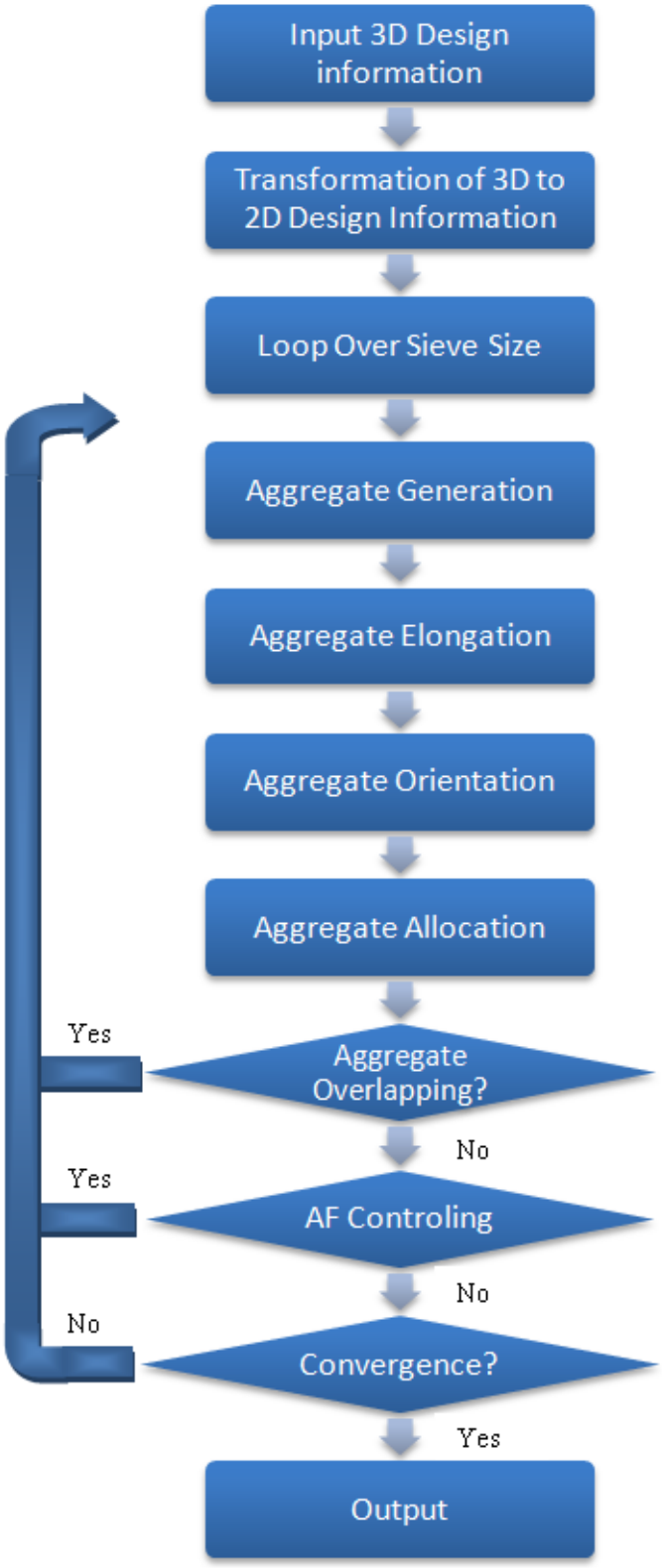

Figure 2.17 Flowchart of the virtual microstructure generation.

The procedure presented above and transformation algorithms developed for converting the 3D volumetric inputs into the 2D characteristics of individual geometric parameters are implemented into virtual microstructure generator software, namely *VMG 1.0*, which was originally developed by Souza (2009). Figure 2.18 shows the interface of the software. By inputting the virtual microstructure type (either rectangular or circular), dimension of the microstructure, 3D volume fraction of aggregates, 3D gradation of aggregates, and AIMS aggregate angularity, *VMG 1.0* can generate the graphical 2D virtual microstructure image with data files. *VMG 1.0* was written using C^{++} language based on object oriented programming.

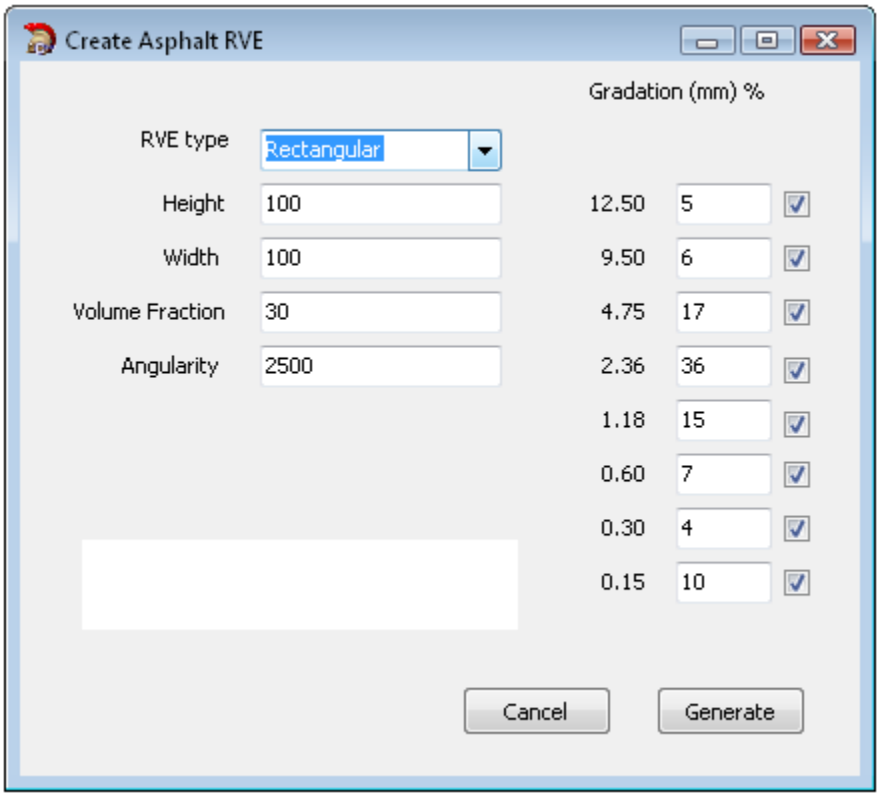

Figure 2.18 Interface of the software, VMG 1.0.

CHAPTER 3

VALIDATION OF VIRTUAL MICROSTRUCTURE

The validation of the virtual microstructure generator developed in this study is presented in this chapter. Among various possible approaches, this study adopted the validation by comparing outputs resulting from the virtual microstructure generator and analysis results obtained from real cross-sectional images of asphalt mixtures with the same geometric inputs, such as 3D gradation, volume fraction, AIMS angularity, aspect ratio, and orientation of aggregate particles. To that end, a typical asphalt concrete mixture was selected for this study, and its geometric inputs necessary for the virtual generation are summarized in Table 3.1.

Table 3.1 Geometric inputs of the asphalt mixture selected in this study for validation.

Geometric Characteristic		Values (Inputs)							
3D Aggregate Gradation	Sieve Size (mm)	19.0	12.7	9.51	4.75	2.38	1.19	0.60	0.30
	AMLP	-	26.25	19.95	12.35	5.66	3.54	-	-
	C	-	2.10	2.10	2.60	2.40	3.00	-	-
	% Passing	100	95	89	72	36	17	7	4
3D Aggregate Volume Fraction		17.9%							
AIMS Aggregate Angularity		2779							
Aggregate Elongation (*AR*)		Uniform distribution of *AR* (1 to 2)							
Aggregate Orientation (θ)		Cumulative distribution curve (Figure 2.15)							

Using the geometric inputs, a total of six virtual microstructure images were generated, and they were compared with the same number of real cross-sectional microstructure images obtained from the mixture sample compacted. To conduct image analyses of the microstructures, a well-known shareware, *ImageTool* (Wilcox, Dove, McDavid, & Greer, 2002), was used. Image analysis results of the virtual and real images were then statistically compared to determine whether those two approaches yield

statistically identical microstructure characteristics. A good agreement between the two approaches indicates that the virtual microstructure generator has been well developed and can potentially replace the physical fabrication and testing of asphaltic mixtures, which can lead to significant time and cost savings. Figure 3.1 illustrates the overall process of the validation effort adopted in this study.

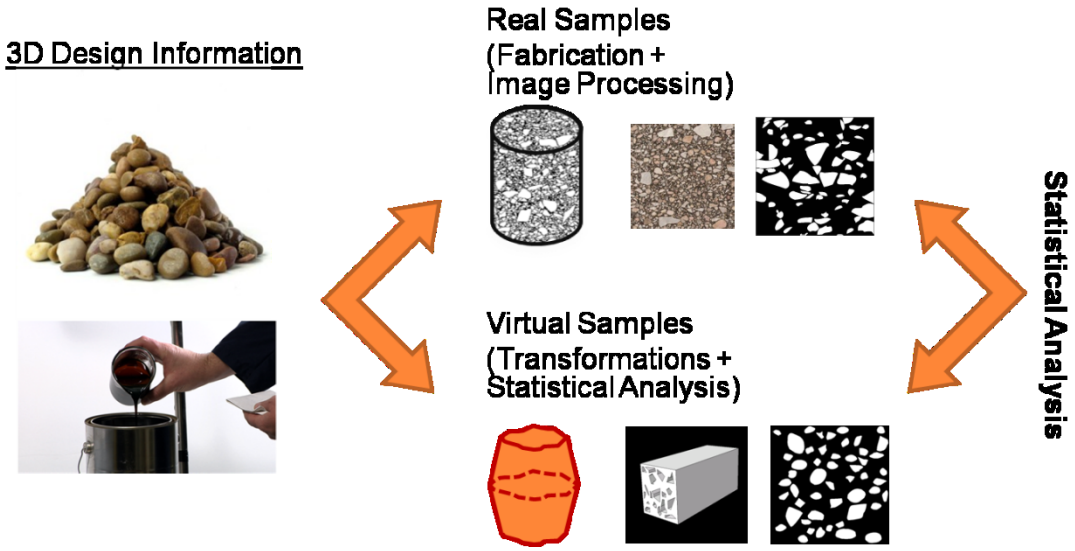

Figure 3.1 Overall process of the validation effort adopted in this study.

3.1. MICROSTRUCTURE IMAGES: REAL AND VIRTUAL

As mentioned earlier, the asphalt mixture was compacted using a Superpave gyratory compactor to produce asphalt concrete samples (150mm in diameter and 175mm in height). The compacted sample was cut vertically using a diamond saw, and the vertical section was placed on a high-resolution scanner to capture inner microstructure images. The virgin inner microstructure image was then processed with sequential image analysis stages as proposed by Papagiannakis et al. (2002). Each surface of the asphalt samples was digitally scanned at a resolution of 100 pixels per inch, where a pixel is defined as

the smallest square unit with the same length on each side. At a resolution of 100 pixels per inch, each pixel was 0.25×0.25 mm^2 in size. The original scanned images of the asphalt mixture samples were then cropped to a length of 90mm and a width of 90mm to make edges clearer, as presented in Figure 3.2(a). The two-dimensional original color images were converted into black and white images by defining a threshold level to identify two separate phases: coarse aggregates in white and the asphalt matrix phase in black (as shown in Figure 3.2(b)). The black and white images of the mixture microstructure required further treatment, since a number of boundaries between the coarse aggregates and the asphalt matrix were indistinguishable, which was not the case in the original images. This blurring typically occurs during the image conversion process. Therefore, thin boundaries were drawn manually between the aggregates and the matrix phase by comparing the black and white image with the color image. This process was performed with great care so as not to violate the mixture microstructure characteristics, such as gradation, orientation, and angularity. Figure 3.2(c) shows a final black and white image after the treatment of unclear aggregate boundaries was completed. The treated image was then finally converted to an image in which fine aggregates (passing No.4 sieve) were removed as shown in Figure 3.2(d). This process was intended for better comparison with results from the virtual microstructure generator, which is limited to representing the actual level of aggregate area fraction and fineness at the current stage of development. Figure 3.3 presents all six real microstructures after image treatment.

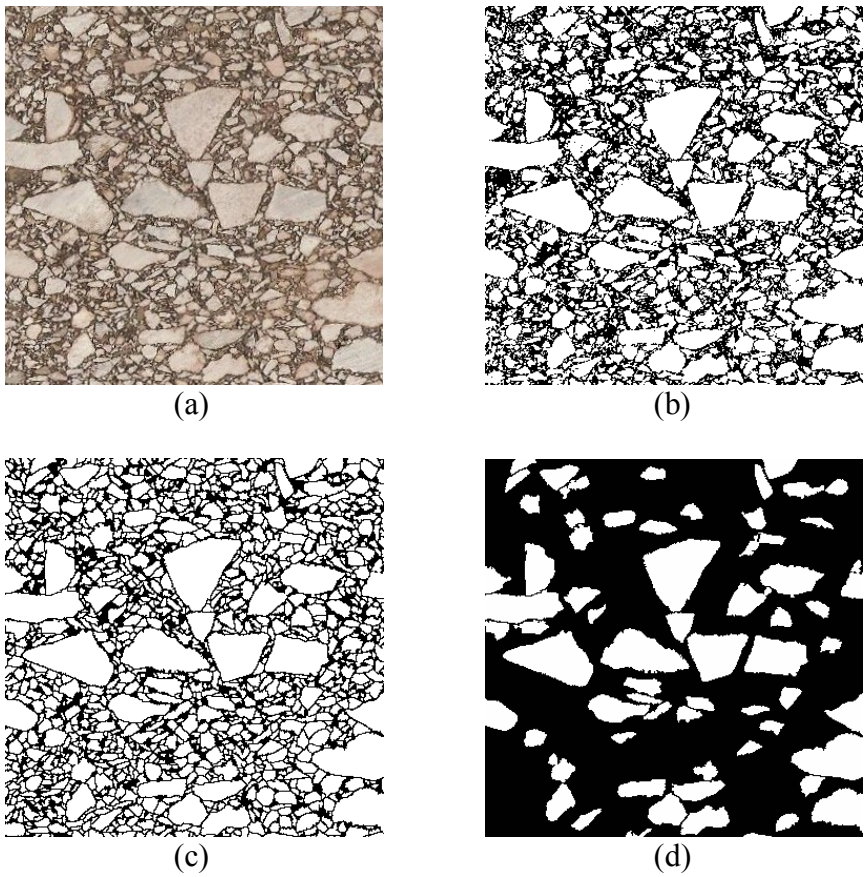

Figure 3.2 Digital image acquisition process of asphalt microstructure: (a) original scanned color image; (b) untreated black and white image; (c) treated black and white image; (d) final black and white image without fine aggregates.

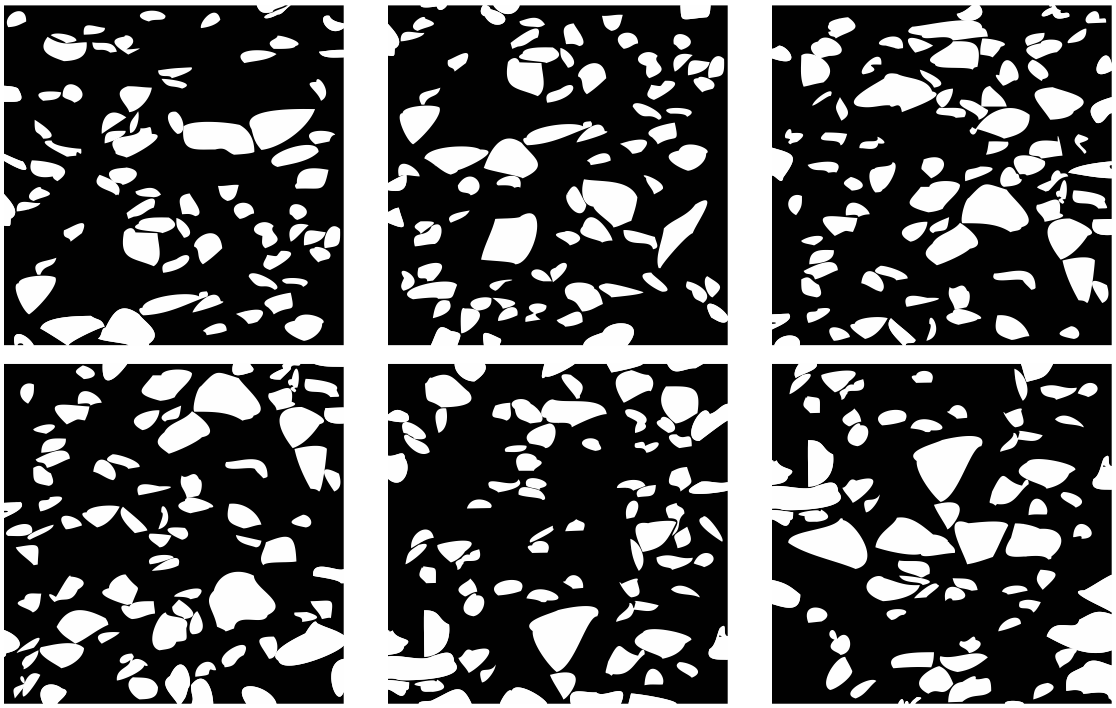

Figure 3.3 Six real microstructure images obtained from the asphalt mixture.

For comparison with the real microstructure images, the same number (six) of images were then produced using the virtual microstructure generator, *VMG 1.0*, with the geometric inputs presented in Table 3.1. Since the validation is based on statistical analysis as mentioned earlier and is discussed later in more detail, a large number of images would be preferred in order to reach more representative findings and conclusions; however, this study utilized the six images because of limited time. Figure 3.4 presents the six microstructure images virtually generated from *VMG 1.0*.

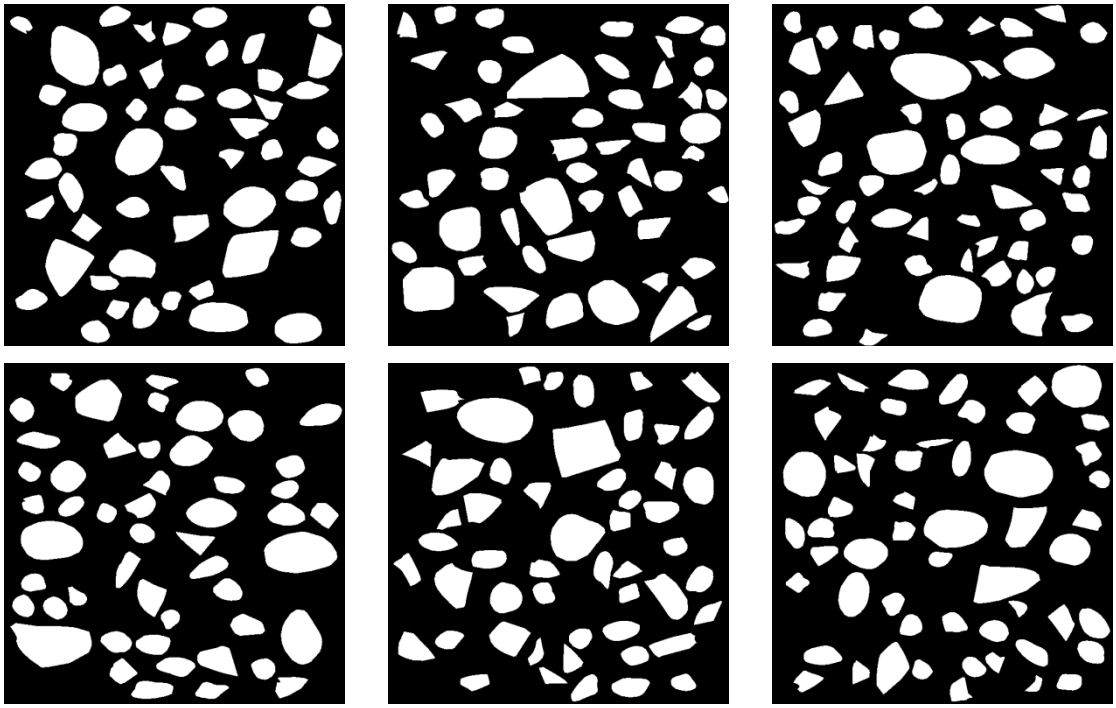

Figure 3.4 Six virtual microstructure images generated from VMG 1.0.

3.2. IMAGE ANALYSIS AND POST-PROCESSING

For both real and virtual microstructure images, the shareware *ImageTool* was used to identify the geometric characteristics of aggregate particles in the images so that the overall microstructure characteristics of the real and virtual images could be compared. *ImageTool* can recognize individual particles and identify various geometric characteristics of each particle, such as the area (a), the major axis (l_M), the minor axis (l_m), the angle of the major axis from horizontal line (θ_M), the angle of the minor axis from horizontal line (θ_m), and coordinates (X_i, Y_i) at corners (i) of the particle boundary.

From the five geometric values of aggregates, the aggregate area fraction (AF), aspect ratio (AR) of aggregates, and orientation of aggregates can be easily identified by estimating the percentage of the area occupied by aggregates, the ratio of major axis (l_M)

to minor axis (l_m), and the angle of the major axis from the horizontal line (θ_M), respectively. Therefore, those three microstructure characteristics (i.e., area fraction, elongation, and orientation of aggregate particles in the mixture) from the virtual generation can be easily validated.

Regarding the validation of aggregate gradation, this study attempted a new post-processing approach for more accurate evaluation. Similar studies (Masad et al.1999; Kim et al. 2009; Karki 2010; Kim et al. 2010; Aragao 2011; Lutif 2011) have performed 2D sieve analysis of cross-sections with simplified methods, such as comparing the length of the major axis or the area of particles with sieve eyes. The results of those simplified approaches do not accurately match with the actual 2D gradation of the mixtures because of the irregular shapes of aggregates. The new approach proposed in this study converts actual irregular-shaped aggregate particles into a simple geometry to perform the sieve analysis without violating the passing/retaining criterion.

Figure 3.5 illustrates the new post-processing approach for aggregate gradation. As shown in the figure, an aggregate is modeled as a general ellipsoidal particle (Figure 3.5(a)). Then, the particle shape at the end of the major axis and the length of the major axis play a significant role in affecting passing (or being retained on) the sieve eye, while the shape in the middle of the particle does not change its gradation. The ellipsoidal particle is then converted into an ideal geometry which is composed of a rectangle and two semicircles attached to both ends of the rectangle, as shown in Figure 3.5(b). The ideal particle geometry in Figure 3.5(b) is not different from the general aggregate shape, Figure 3.5(a) in terms of its gradation; therefore, the ideal particle can be used to check its gradation characteristics. Two lengths are required to define the ideal particle: the

length of the major axis (l_M) and the diameter of the semicircles which is equal to the length of the minor axis (l_m) of the ideal particle.

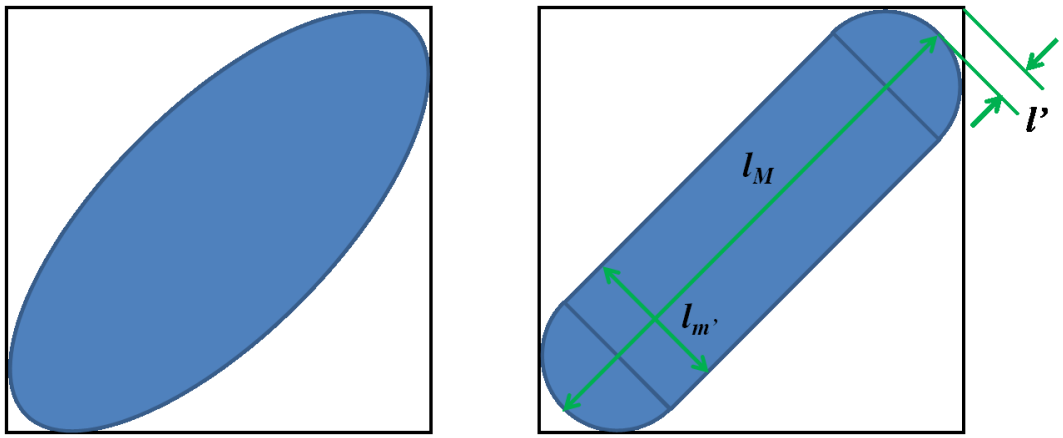

Figure 3.5 New post-processing approach for aggregate gradation analysis.

In the gradation analysis, the diagonal length of the square, which is in contact with the ideal particle shown in Figure 3.5(b), is estimated and compared to the diagonal length of sieve eyes to determine if the particle passes or is retained on the sieve. The diagonal length of the square, denoted herein as Length Index (*LI*), can be calculated geometrically by using the aggregate geometry information (l_M, l_m, θ_M, and θ_m) obtained from the *ImageTool* analysis. A finally derived equation can be written as follows:

$$LI = l_M + 2l' = l_M + l_m\left(\sqrt{2}-1\right)\cos\left(\left|\theta_m - \theta_M\right|\right) \qquad [3.1]$$

Lastly, the angularity of aggregates is an important geometric property that needs to be estimated to validate the quality of *VMG 1.0*. As mentioned earlier, AIMS

angularity is used as an input in *VMG 1.0*, but a different angularity index based on 40 edge points was implemented in the software to represent the target AIMS angularity. This is because the 40-point angularity index, although it is approximate, presents a strong relationship with the AIMS angularity (Souza 2009) and can sufficiently simulate the realistic characteristics of aggregate angularity in actual mixtures with much less computational effort.

Using the *ImageTool* analysis results (i.e., coordinates (X_i, Y_i) identified at sharp corners (i) of an arbitrary aggregate particle), average angularity index (*AAI*) was calculated to equivalently compare the angularity characteristics of aggregates represented by virtual images and real microstructures. *AAI* represents aggregate angularity by taking an average of angles from gradient vectors (ϕ_i) at sharp corners, instead of taking the summation of the angles from gradient vectors at corners as the AIMS estimates. This is beneficial to removing the effects of image resolution and the number of edge points selected per particle. The following expression is used to calculate *AAI*.

$$AAI = \frac{\sum_{j=1}^{m}\sum_{i=1}^{n}\phi_{ij}}{\sum_{j=1}^{m} n_j} \qquad [3.2]$$

where ϕ_{ij} = gradient vector at ith corner of jth particle;

m = total number of particles analyzed; and

n = total number of corners of jth particle.

To check the validity of the new angularity index (*AAI*) for post-processing, *AAI* values were compared to the 40-point angularity index values with the same aggregate particles. As expected and as demonstrated in Figure 3.6, both indices are correlated with a strong linear relationship, which implies that the use of *AAI* is appropriate for validation of the virtual microstructure generator in terms aggregate angularity.

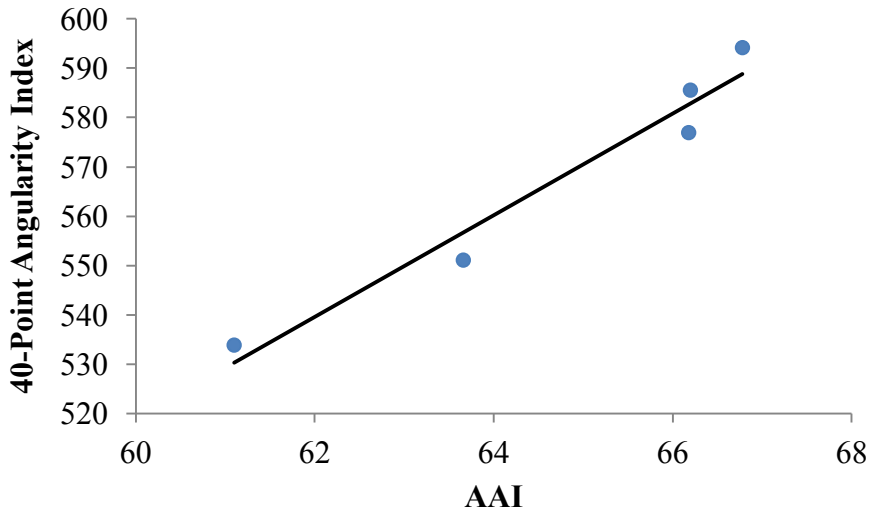

Figure 3.6 Relationship between AAI and 40-point angularity index.

3.2. ANALYSIS RESULTS AND DISCUSSION

Analysis results of individual images from the real and virtual microstructures are summarized in Table 3.2. Mean values and standard deviations of each case are also presented in the table for statistical analyses. Since the number of samples for each case is limited to only six with normal distributions assumed, the Student ***t***-test was selected to perform statistical analysis comparing real and virtual microstructures. The null hypothesis for this test is $\mu 1 - \mu 2 = 0$ (or $\mu 1 = \mu 2$) against $\mu 1 <> \mu 2$ with a 0.5% significance level. If the ***P***-value (Pr. > |***t***|) is less than the significance level, the null hypothesis is rejected and it is concluded that the two mean values are significantly

different. The results of the statistical analysis are presented in Table 3.3. As can be seen in the table, all of the null hypotheses except the elongation were accepted, which indicates that geometric characteristics between the virtual microstructures and real microstructures are statistically identical for various geometrical characteristics excluding the aggregate elongation with a significance level of 0.5%. The assumption made to aggregate elongation in the previous studies was not valid. It further demonstrates that the new 3D-2D transformation algorithms were properly developed and implemented into the virtual microstructure generator, *VMG 1.0*.

Table 3.2 Image analysis results: real microstructures vs. virtual microstructures.

Geometric Characteristics		1	2	3	4	5	6	Mean	St. Dv.
2D Aggregate Gradation	Sieve Size	Real Microstructure Images							
	12.7mm	25.4	28.6	18.8	19.0	21.2	46.4	26.6	10.5
	9.51mm	15.5	14.3	20.9	23.7	27.0	13.1	19.1	5.6
	4.75mm	59.2	57.0	60.3	57.4	51.8	40.5	54.4	7.4
	Sieve Size	Virtual Microstructure Images							
	12.7mm	32.4	28.7	27.8	25.8	26.5	24.8	27.7	2.7
	9.51mm	15.2	19.6	16.1	20.8	19.2	21.5	18.7	2.5
	4.75mm	52.3	51.7	56.0	53.5	54.3	53.2	53.5	1.5
Aggregate Area Fraction (*AF*)		Real Microstructure Images							
		23.1	25.3	28.9	29.1	26.5	29.3	27.0	2.5
		Virtual Microstructure Images							
		28.0	28.1	26.8	28.2	27.7	27.5	27.5	0.5
Aggregate Angularity (*AAI*)		Real Microstructure Images							
		61.2	64.7	63.5	65.8	66.4	66.0	64.6	2.0
		Virtual Microstructure Images							
		66.1	64.1	61.5	64.5	66.8	66.4	64.9	2.0
Aggregate Orientation (θ)		Real Microstructure Images							
		31.3	28.6	30.7	29.4	27.3	31.3	29.8	1.6
		Virtual Microstructure Images							
		30.2	29.1	33.6	20.3	33.3	33.8	30.1	5.2
Aggregate Elongation (*AR*)		Real Microstructure Images							
		2.44	2.27	2.11	2.44	2.27	2.23	2.29	0.13
		Virtual Microstructure Images							
		1.58	1.66	1.63	1.57	1.66	1.63	1.62	0.04

Table 3.3 Statistical analysis results.

Geometric Characteristics		***t*-test**	***P*-value (Pr. > |*t*|)**	**H_o Status**
2D Aggregate Gradation	% passing 12.7mm sieve	0.013	0.9896	Accepted
	% passing 9.51mm sieve	0.190	0.8520	Accepted
	% passing 4.75mm sieve	0.146	0.8860	Accepted
Aggregate Area Fraction (*AF*)		0.111	0.9132	Accepted
Aggregate Angularity (*AAI*)		0.049	0.9613	Accepted
Aggregate Orientation (θ)		0.092	0.9279	Accepted
Aggregate Elongation (*AR*)		7.65	0.00002	Rejected

CHAPTER 4

SUMMARY AND CONCLUSIONS

This thesis describes the development and validation of a virtual generation method for mixture microstructures along with post-processing methods of microstructure images. These methods were developed so that virtual generation can potentially replace the physical fabrication and testing of asphaltic mixtures. In order to accurately represent the geometric characteristics of real microstructures, virtual fabrication incorporated new 3D-2D transformation algorithms for several geometrical properties of aggregates, such as gradation, angularity, and aspect ratio, into the virtual microstructure generator. 3D volume fraction and orientation of aggregates in the mixture were also converted to 2D characteristics to appropriately simulate complex microstructure characteristics. For validation, the virtually-generated microstructures were compared to real cross-sectional microstructure images obtained from actual samples, which presented a good agreement between the virtual and real microstructures. The good agreement demonstrates that the new 3D-2D transformation algorithms were properly developed and implemented into the virtual microstructure generator, *VMG 1.0*.

Further advancements, such as the consideration of air voids as a separate phase, the better representation of particle elongation in the mixture, the consideration of variances in the statistical analyses, and the extension of the 2D microstructure to the actual 3D virtual fabrication, are necessary to improve the virtual fabrication and evaluation of mixtures. For this study, only a limited number of samples for one mixture were used for validation. To reach general conclusions, this clearly needs further

investigation with more cases and different types of mixtures. Although much future work is required, the current development is at least sufficient to demonstrate the benefits and potential of this effort. Virtual fabrication and testing can result in significant time and cost savings compared to more expensive and repetitive laboratory fabrication and performance tests of actual specimens. Furthermore, microstructure generation can be incorporated into various computational approaches to microstructure characterization and performance modeling with much less laboratory effort than conventional phenomenological-experimental approaches.

REFERENCES

Abbas, A., Masad, E., Papagiannakis, T., & Shenoy, A. (2005). Modeling asphalt mastic stiffness using discrete element analysis and micromechanics-based models. *International Journal of Pavement Engineering, 6*(2), 137-146.

Al-Rousan, T., Masad, E., Myers, L., & Spiegelman, C. (2005). A new methodology for shape classification of aggregates. *Journal of the Transportation, 1913*, 11-23.

Ammouche, A., Breysse, D., Hornain, H., Didry, O., & Marchand, J. (2000). A new image analysis technique for the quantitative assessment of microcracks in cement-based materials. *Cement and Concrete Research, 30*(1), 25-35.

Andrei, D., Witczak, M. W., & Mirza, M. W. (1999). *Development of a revised predictive model for the dynamic (complex) modulus of asphalt mixtures.* College Park, MD: University of Maryland.

Aragao, F. T. (2011). Computational microstructure modeling of asphalt mixtures subjected to rate-dependent fracture . *PhD dissertation*. Lincoln, NE: University of Nebraska-Lincoln.

Aragao, F. T., & Kim, Y. (2010). Modeling of asphaltic materials subjected to nonlinear viscoelastic fracture. *Geo Florida Conference of the American Society of Civil Engineers* (pp. 2662 - 2671). West Palm Beach, FL: ASCE.

Aragao, F. T., & Kim, Y. (2011). Characterization of fracture properties of asphalt mixtures based on cohesive zone modeling and digital image correlation

technique. *Transportation Research Board* (pp. 11-1229). Washington, D.C: National Research Council.

Aragao, F. T., Kim, Y., Karki, P., & and Little, D. N. (2010). Semi - empirical, analytical, and computational predictions of dynamic modulus of asphalt concrete mixtures. *Journal of the Transportation Research Board, 2181*, 19-27.

Aragao, F. T., Kim, Y., Lee, J., & Allen, D. H. (2011). Micromechanical model for heterogeneous asphalt concrete mixtures subjected to fracture failure. *Journal of Materials in Civil Engineering, 23*(1), 30-38.

ASSHTO T326. (2008). *Standard Method of Test for Uncompacted Void Content of Coarse Aggregate (As Influenced by Particle Shape , Surface Texture, and Grading)*. Washington, D.C.: ASSHTO.

ASTM D5821. (2006). *Standard Test Method for Determining the Percentage of Fractured Particles in Coarse Aggregate.* West Conshohocken, PA: ASTM .

Ballani, F. (2005). A case study: Modeling of self-flowing castables based on reconstructed 3D images. *9th Eur. Congr. Stereol. Image Anal.* (pp. 282-288). Krakow.: Polish Soc. Stereol.

Bari, J., & Witczak, M. W. (2006). Development of a new revised version of the Witczak E* predictive model for hot mix asphalt mixtures. *Journal of the Association of Asphalt Paving Technologists, 75*, 381-423.

Bentz, D. P., Garboczi, E. J., & Stutzman, P. E. (1993). Computer modeling of the interfacial transition zone in concrete. *Interfaces in Cementitious Composites* (pp. 107–116). London: NIST.

Brandes, H. G., & Hirata, J. G. (2009). An automated image analysis procedure to evaluate compacted asphalt section. *International Journal of Pavement Engineering, 10*(2), 87-100.

Breugel, K. V. (1991). Simulation of hydration and formation of structure in hardening cement-based materials. *PhD Dissertation*. DUP: Delft.

Brzezichi, J. M., & Kasperkiewicz, J. (1999). Automatic image analysis in evaluation of aggregate shape. *Journal of Computing in Civil Engineering, 13*(2), 123-128.

Bullard, J. W., Ferraris, C. F., Garboczi, E. J., Martys, N. S., & Stutzman, P. A. (2004). Virtual cement and concrete. In *Innovations in Portland Cement Manufacturing* (pp. 1311-1331). Skokie, IL: National Institude of Standards and Technology.

Chandan, C., Sivakumar, K., Masad, E., & Fletcher, T. (2004). Application of imaging techniques to geometry analysis of aggregate particles. *Journal of computing in Civil Engineering, 18*(1), 75-82.

Christensen, D. W., Pellinen, T., & Bonaquist, R. F. (2003). Hirsch model for estimating the modulus of asphalt concrete. *Journal of the Association of Asphalt Paving Technologists, 72*, 97-121.

Christensen, R. M. (1982). *Theory of viscoelasticity: An introduction.* New york: Academic.

Dai, Q., & You, Z. (2007). Prediction of creep stiffness of asphalt mixture and micromechanics finite-element and discrete models. *Journal of Engineering Mechanics, 133*(2), 163-173.

Diekamper, R. (1984). Technische wissenschaftliche mitteilungen der Inst. für konstruktiven ingenieursbau. Ruhr Universität Bochem.

Espinosa, H. D., & Zavattieri, P. D. (2003). A grain level model for the study of failure initiation and evolution in polycrystalline brittle materials. *Mechanic of Material, 35*(3-6), 333–364.

Freitas, F. A. (2007). A theoretical and experimental technique to measure fracture properties in viscoelastic solids. *Ph.D. Dissertation*. Lincoln, NE: University of Nebraska-Lincoln.

Geubelle, P. H., & Baylor, J. S. (1998). Impact-induced delamination of composites: A 2D simulation. *Composites, 29*, 589-602.

Gudimettla, J., Myers, L. A., & Paugh, C. (2009). *AIMS: The future in rapid, automated aggregate shape and texture measurement.* Grove City, PA: Pine Instrument Company.

Higgins, M. D. (2000). Measurement of crystal size distribution. *American Mineralogist, 85*(9), 1105-1116.

Hu, J., & Stroeven, P. (2006). Shape characterization of concrete aggregate. *Image Analysis and Stereology, 25*(1), 43-53.

Jähne, B. (1997). *Practical handbook on image processing for scientific applications.* Boca Raton, Fla.: CRC-Press.

Karki, P. (2010). Computational and experimental characterization of bituminous composites based on experimentally determined properties of constituents. *Master Thesis*. Lincoln, NE: University of Nebraska-Lincoln.

Khanna, S. K., Ranganathan, P., Yedla, S. B., Winter, R. M., & Paruchuri, K. (2003). Investigation of nanomechanical properties of the interphase in a glass fiber reinforced polyester composite using nanoindentation. *Journal of Engineering Materials and Technology, 125*(2), 90-96.

Kim, Y., Aragao, F. T., Allen, D. H., & Littled, D. N. (2010a). Damage modeling of bituminous mixtures considering mixture microstructure, viscoelasticity, and cohesive zone fracture. *Canadian Journal of Civil Engineering, 37*(8), 1125-1136.

Kim, Y., Karki, P., & Im, S. (2010b). Dynamic modulus prediction of asphalt concrete mixture through mixture microstructure characteristics and mechanical properties of constituents. *Transportation Research Record.* Washangton DC: Paper Submitted.

Kim, Y., Lee, J., & Lutif, J. S. (2010c). Geometrical evaluation and experimental verification to determine representative volume elements of heterogeneous asphalt mixtures. *Journal of Testing and Evaluation, 38*(6), 30-38.

Kim, Y., Little, D. N., & Lytton, R. L. (2003). Fatigue and healing characterization of asphalt mixtures. *Journal of Materials in Civil Engineering, 15*(1), 75-83.

Kim, Y., Lutif, J. S., & Allen, D. H. (2009). Determination of representative volume elements of asphalt concrete mixtures and their numerical validation through finite element method. *Journal of Transportation Research Board, 2127*, 52-59.

Kwan, A. K., Mora, C. F., & Chan, H. C. (1999). Particle shape analysis of coarse aggregate using digital image processing. *Cement and Concrete Research, 29*(9), 1403-1410.

Li, L., Chan, P., Zollinger, D. G., & Lytton, R. L. (1993). Quantitative analysis of aggregate shape based on fractals. *ACI Materials Journal, 90*(4), 357-365.

Lutif, J. S. (2011). Computational micromechanics modeling of damage-dependent bituminous composites based on two-way coupled multi-scale approach . *PhD dissertation*. Lincoln, NE: University of Nebraska-Lincoln.

Marinoni, N., Pavese, A., Foi, M., & Trombino, L. (2005). Characterisation of mortar morphology in thin section by digital image processing. *Cement and Concrete Research, 35*(8), 1613-1619.

Masad, E. (2003). *The development of a computer controlled image analysis system for measuring aggregate shape properties.* Washington, D.C.: National Cooperative Highway Research Program NCHRP-IDEA Project 77 Final Report, Transportation Research Board, National Research Council,.

Masad, E., Muhunthan, B., Shashidhar, N., & Harman, T. (1999). Internal structure characterization of asphalt concrete using image analysis. *Journal of Computing in Civil Engineering, 13*(2), 88-95.

Masad, E., Niranjanan, S., Bahia, H., & Kose, S. (2001). Modeling and experimental measurements of localized strain distribution in asphalt mixes. *Journal of Transportation Engineering, 127*(6), 477-485.

Meakawa, K. C., & Kishi, T. (1999). Modeling of concrete performance-hydration. *Micro-Structure Formation and Mass Transport.* London: E&FN Spon.

MEPDG. (2003). Design of new and rehabilitated pavement structures. *Design Guide*. National Cooperative Highway Research Program.

Mora, C. F., Kwan, A., & Chan, H. C. (1998). Particle size distribution analysis of coarse aggregate uding digital image processing. *Cement and Concrete Research, 28*(6), 921-932.

Oliver, W. C., & Pharr, G. M. (1992). An improved technique for determining hardness and elastic modulus using load and displacement sensing indentation experiments. *Journal of Materials Research, 7*(6), 1564.

Papagiannakis, A. T., Abbas, A., & Masad, E. (2002). Micromechanics analysis of viscoelastic properties of asphalt concretes. *Journal of the Transportation Research Record, 1789*, 113-120.

Peterson, T. D. (1996). A refined technique for measuring crystal size distributions in thin section. *Contrib Mineral Petrol, 124*(3-4), 395-405.

ROELFSTRA, P. E. (1989). A numerical approach to investigate the properties of numerical concrete. *PhD Dissertation*. Lausanne: EPFL-Lausanne.

Schapery, R. A. (1984). Correspondence principles and a generalized J-integral for large deformation and fracture analysis of viscoelastic media. *International Journal of Fracture, 25*(3), 195–223.

Shin, S., & Hryciw, R. D. (2004). Wavelet analysis of soil mass image for particle size determination. *Journal of Computing in Civil Engineering, 18*(1), 19-27.

Simulia. (2009). *Abaqus/CAE User's Manual.* Providence, RI: Dassault Systèmes Simulia Corp.

Song, S. H., Paulino, G. H., & Buttlar, W. G. (2006). A bilinear cohesive zone model tailored for fracture of asphalt concrete considering viscoelastic bilk material. *Engineering Fracture Mechanics, 73*(18), 2829–2848.

Souza, L. T. (2009). Investigation of aggregate angularity effects on asphalt concrete mixture performance using experimental and virtual asphalt samples. *Master Thesis*. Lincoln, NE: University of Nebraska-Lincoln.

Stroeven, P. (1973). Some aspects of the micro-mechanics of concrete. *PhD Dissertation*. DUT, Delft.

Stroeven, P., Sluys, L. J., Guo, Z., & Stroeven, M. (2006). Virtual reality studies of concrete. *Forma*, 227-242.

Underwood, E. E. (1970). *Quantitative stereology.* Addison-Wesley Publishing Company.

Wicksell, S. D. (1925). The corpuscle problem: A mathematical study of a biometric. *Biometrika*, 84-99.

Wilcox, C. D., Dove, S. B., McDavid, W. D., & Greer, D. B. (2002). ImageTool. San Antonio, Texas: Department of Dental Diagnostic Science at The University of Texas Health Science Center.

Williams, S. R., & Philipse, A. P. (2003). Random packings of spheres and spherocylinders simulated by mechanical contraction. *Physical Review, 67*(5), 1-9.

Witczak, M. W., & Bari, J. (2004). *Development of a E* master curve database for lime modified.* Tempe, AZ: Arizona State University.

You, Z., & Buttlar, W. G. (2006). Micromechanical modeling approach to predict compressive dynamic moduli of asphalt mixture using the distinct element method. *Journal of the Transportation Research Record, 1970*, 73-83.

You, Z., Adhikari, S., & Kutay, M. E. (2009). Dynamic modulus simulation of the asphalt concrete using the X-ray computed tomography images. *Materials and Structures, 42*(5), 617-630.

You, Z., Bekking, W., & Morin, I. (1995). Application of digital image processing to quantitative study of asphalt concrete microstructure. *Journal of the Transportation Research Record, 1492*, 53-60.

Zaitsev, J. W., & Wittmann, F. H. (1977). *Crack propagation in a two-phase material such as concrete, in Fracture.* Waterloo, Canada: ICF4.

Zelelew, H. M., Papagiannakis, A. T., & Masad, E. (2008). Application of digital image processing techniques for asphalt concrete mixture images. *The 12th International*

Conference of International Association for Computer Methods and Advances in Geomechanics (pp. 119-124). Goa, India: International Association for Computer Methods and Advances in Geomechanics.

Zhang, P. (2003). Microstructure generation of asphalt concrete and lattice modeling of its cracking behavior under low temperature. *Ph.D. dissertation*. Raleigh, NC: North Carolina State University.